Structural Improvements of a FishBAC Design

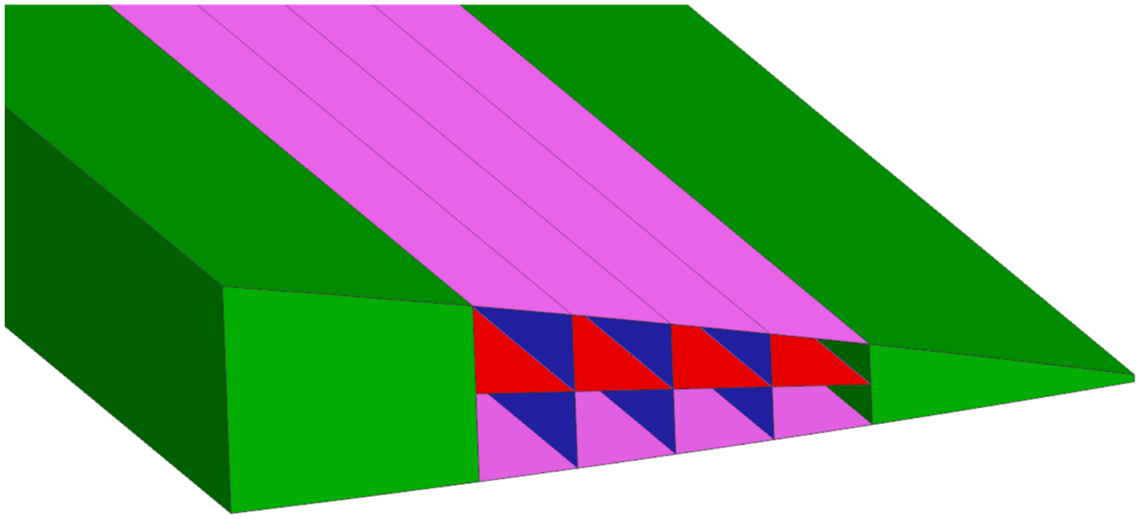

Author: **ALFAL/ENGAER 139923-D Tiago Emanuel Pereira Nunes**
Master of Science Degree in Military and Aeronautical Sciences - Aeronautical Engineering
Air Force Academy, Sintra

Supervisor: **Prof. Benjamin King Sutton Woods**
Bristol University

Co-supervisor: **TCOR/ENGAER 129905-A Luís Filipe da Silva Félix**
Air Force Academy, Sintra

Abstract

The aeronautical industry is well known for its high demands. Nowadays, the demands are higher and more visible, which leads to the active search for new ideas and solutions that are innovative, creative and more efficient for the continuous evolution of the aircraft's performance. One of these new and promising ideas is the Fish Bone Active Camber (FishBAC) wing, which is a type of camber morphing wing. This dissertation work proposes new solutions that aim to mitigate the limitations of the current models of the FishBAC technology. As a compliance-based morphing mechanism, the distribution and orientation of stiffness within the FishBAC are incredibly important. The overall goal is to achieve high compliance in the camber morphing direction while maintaining high stiffness in the other directions. The geometry of the FishBAC is designed to create a high level of structural anisotropy. This work seeks to push this structure further by investigating a series of design changes that will further augment the material and geometric anisotropy in order to increase the performance of the FishBAC. These solutions were obtained using three different models. The first model presents a spine with rectangular cutouts. The second one has Carbon Fibre Reinforced Polymer (CFRP) pultrusions attached to the stringers next to the skin. The third model combines the characteristics of the other two. The results obtained through the Finite Element Analysis (FEA) for these models, were compared to a basic FishBAC model with no modifications. This process helped to conclude, that cutouts have a positive effect in diminishing the stiffness of the model with a modest impact in deflection variation along the wingspan. The CFRP pultrusions have been demonstrated to be much less effective to respond to this deflection variation problem than it was expected.

Keywords: FEA, CAD, Morphing Wing, FishBAC, CFRP.

1 Introduction

Camber morphing wings are a promising way of accomplishing the performance needs of an aircraft since these structures are much more aerodynamic efficient than conventional devices, such as ailerons or elevators (Rivero, Fournier, Manolesos, Cooper, & Woods, 2020). This can provide the lift needed for different stages of aircraft operations with less drag and noise, usually associated with hinged control panels (Rivero, Weaver, Cooper, & Woods, 2018).

Another advantage of employing camber morphing devices is that it can be utilised actively during flight, to optimise the span-wise lift distribution (Rivero et al., 2018). It is also of relevant interest that this kind of technology has the potential to significantly reduce the environmental impact of the aviation sector, by reducing fuel consumption (Greff, 1990 and Burdette & Martins, 2019).

Several devices and designs have been tested over the years and, the FishBAC illustrated in Figure 1, developed by Woods and Friswell (2012), is one idea that has shown potential to be further studied due to the promising aerodynamic results and the developments that have been presented in the terms of manufacturability (Rivero, Fournier, Heeb, & Woods, 2022).

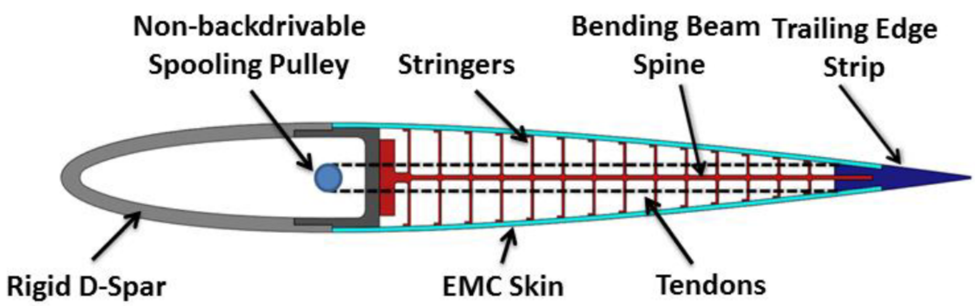

Figure 1: Aerofoil view of the Fish Bone Active Camber concept (Woods & Friswell, 2013).

As Rivero et al. (2022) considered, the first generation of FishBAC devices had a 3D single internal "skeleton", constituted by the stringers and the spine, that was printed in one single piece made of Acrylonitrile Butadiene Styrene (ABS) plastic. Then, a silicone elastomer skin was further pre-stretched and glued to this skeleton, while the pulley mechanisms were produced separately and added subsequently.

Following the classification made by Rivero et al. (2022), the second generation of FishBAC devices was designed with the main objective to include carbon fiber-reinforced composite into the spine. This material has much better structural qualities than 3D-printed plastics, and it also enables this structural part to have the desired stiffness according to the differences in fiber angle in each ply of the composite (Rivero, Fournier, Weaver, Cooper, & Woods, 2018). As was also the case for the first generation, this second one demonstrated the obvious aerodynamic advantages that this camber morphing mechanism has when compared to a conventional hinged trailing-edge flap of similar dimensions (Rivero, Fournier, Manolesos, Cooper, & Woods, 2021).

Finally, a third generation FishBAC was introduced by Rivero et al. (2022). This new design had a much easier removal and repair process, the capacity to do the adjustment of the tension applied to the tendons and the skins and stringers were attached without using any adhesive.

The purpose of this work is, to explore and possibly propose new ideas and concepts that can make the camber morphing mechanism more structurally efficient. The study of structural efficiency will focus on minimising elastic washout between actuation stations, while trying to maintain or even diminish the complexity and total mass of the build. Another goal of this work is to provide computational models and results that support the Finite Element (FE) runs on potential modifications to the FishBAC structure. In order to achieve those objectives, Computer Aided Design (CAD) modeling and FEA will be used in order to evaluate the designed structure and give important information that can support the conducted study.

2 Solutions to study and Decision process

All three generations of the FishBAC have shown one common issue, the elastic washout. This is clearly a problem that needs to be addressed. Conceiving an innovative and efficient solution for this issue can be challenging. There are factors that have to be considered in all aeronautical structures: they must be as lightweight as possible, easy to maintain, have a reduced impact on the environment and, of course, with the lowest cost possible involved.

2.1 Possible ideas

This process of brainstorming ideas and solutions was done considering the third generation of the FishBAC presented by Rivero et al. (2022). For every main component, a different uppercase letter was designated: A - spine; B - stringers; C - skins; D - trailing edge and E - actuation points. At least one idea was found for every component.

The considered ideas were: A1 - Cutouts in the spine plate; B1 - CFRP pultrusions added to the stringer and next to the skin; B2 - Multi-stiffness Thermoplastic polyurethane (TPU) stringers with "compliant hinges"; B3 - Stringer cutouts; C1 - Spanwise reinforcement with stiffeners of TPU/CFRP reinforcement; D1 - CFRP reinforcement with embedded pultrusions; E1 - More actuation points with specific actuation loads.

The idea A1, consists of removing a certain percentage of material from the spine in both chord and spanwise directions. This idea has the purpose of diminishing the overall weight and giving less stiffness to the spine.

The B1 idea has the intention to better distribute the deformation of the stringer along the span, especially, as far as possible from the spine. This is accomplished by creating some attachments that can make room for the CFRP pultrusions to be inserted between the stringer and the skin. The idea B2 is to use a different stringer that has two different materials with different rigidity. These are 3D printed so that a grid is formed by the material that is more rigid and the junctions of the grid are made by the less rigid material, forming the so-called "compliant hinges". The idea B3 is, as mentioned for idea A1, to remove a certain percentage of material but, in this case, for the stringer. The idea C1 is to incorporate structure reinforcements made of CFRP or TPU, along the spanwise direction, placed next to the skin. The idea D1 is similar to the idea B1 but, in this case, the CFRP pultrusions were placed on the trailing edge of the device. The idea E1, consists in adding more actuation points throughout the wing span. In these added actuation stations, an increase in the torque (T) must be applied in a certain way so that the deflections of the tailing edge would be more similar, attenuating the elastic washout effect.

2.2 Decision Process

The decision process began with a selection of different criteria. Seven defined criteria were elaborated in order to better suit the objectives of the current work, tackling the limitations of the FishBAC. Since different defined criteria have different importance weight in the achievement of the objectives of this study, they were rated on a scale from 1 to 5, from the least to the most important, as follows: Criteria 1 - effectiveness to reduce washout, with a rating of 5; Criteria 2 - torsional rigidity, Criteria 3 - the capability to achieve big spanwise deformation and Criteria 4 - risk to achieve the objectives, with a rating of 4; Criteria 5 - complexity of the build; Criteria 6 - the cost of the build, with a rating of 3 and finally, Criteria 7 - easier maintenance of the concept, with a rating of 2.

In the next step of the decision process, the model ideas (7 in total) were classified according to their capacity to achieve what is stated by the criteria. A scale from 1 to 5 was also used, where 1 is given to an idea model that can not fulfill the objective define in a certain criteria and 5 to the model that can easily accomplish it. This assessment was done using personal engineering judgment of the importance of each criteria and idea, resulting in qualitative assessments being turned into a quantitative decision process.

Subsequently, multiplying the criteria ratings by the idea rating a summation of all weighted ratings of each idea model was obtained. This value indicates, in a quantitative way, how a model can deliver a result that can respond to the objectives. Considering this, because of their higher score values, the models A1 and B1 were selected to be further investigated.

3 Baseline model

A baseline model was designed using, as a reference, the third generation of FishBAC designs presented by Rivero et al. (2022). It is a simplified version that includes all major components, namely the skin, spine, stringers and a rigid trailing edge part. This model only represents the section of the wing where the camber morphing part is localised, which starts at 75% of the aerofoil chord. The aerofoil, chord dimensions and span used were the same as the ones used in the third generation of FishBAC designs, presented by Rivero et al. (2022).

3.1 Computer Aided Design (CAD) model

The Siemens NX with the Simcenter Nastran 2020 program, version 1911, was the computational program chosen, not only to elaborate the CAD model but also to perform the FEA.

Firstly, the aerofoil was sketched in 2D, using the reference points delivered by the database in Airfoil Tools (2022). From this 2D sketch, two vertical lines were drawn, one where the morphing part begins at coordinate x normalized by the chord ($x/c = 0.75$) and the other line closer to the leading edge (for $x/c \approx 0.65$). These lines, in addition to the lines that define the 2D aerofoil form the plane that will be later extruded to form the rigid part closest to the leading edge of the wing. In a similar process, another vertical line was drawn at $x/c = 0.9$, defining the limit of the plane that will later generate the trailing edge rigid part. Both of these planes, linked with rigid parts, are seen in Figure 2 (a) with a green colour. Subsequently, a horizontal line, placed in the middle of the aerofoil is defined, beginning at $x/c = 0.75$ and ending at $x/c = 0.9$. This line will later be used to establish the spine of the model. Still, inside the mentioned range ($x/c = 0.75$ and $x/c = 0.9$), three other vertical lines were perfectly distributed, being equally spaced between them and between the limits of the morphing section. These lines were created in order to define the stringer of this design. Finally, the complete 2D sketch is obtained, seen in Figure 2 (a). This profile is then extruded in the normal direction of the plane where it was drawn, forming the 3D CAD. This extrusion was done until the 3D structure had a wingspan of 995 mm.

The final CAD is presented in Figure 2 (b), using the green colour for the representation of the rigid parts, pink colour for the skin, dark blue for the stringers and red for the spine.

3.2 Finite Element Analysis

3.2.1 Mesh, Element types and Material properties

An initial element base size of 3 mm was used for all the components of the CAD. For the 2D surfaces that represent the skin and the stringers, shell elements were used, due to the fact that these types of elements are able to resist bending loads

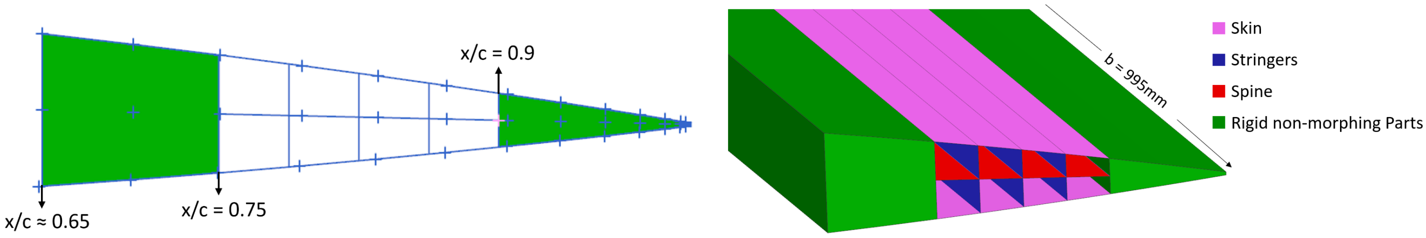

(a) Final 2D sketch for the baseline model CAD.

(b) Isometric perspective of a portion of the baseline model CAD.

Figure 2: Baseline CAD

and they are ideal for modeling thin plates. In terms of the shape of the elements, the CQUAD4 (quadrilateral element with four nodes) was used for the skin, stringers and spine, because all these components have a rectangular-like configuration.

For the rigid and 3D portions of the model, a CHEXA(8) element, that is a six sided solid element, was selected due to the need to capture the complexity of the geometry and the possibility of three-dimensional deformations.

It is also important to mention that, all these elements used are linear since we are developing a Linear Statics FEA. Due to this, is possible to say that, the greater the number of elements involved, the more refined the mesh will be, the better precision in the results is expected to be obtained.

The obtained mesh is represented in Figure 3, where the green elements are the CQUAD4 and the orange ones are CHEXA(8).

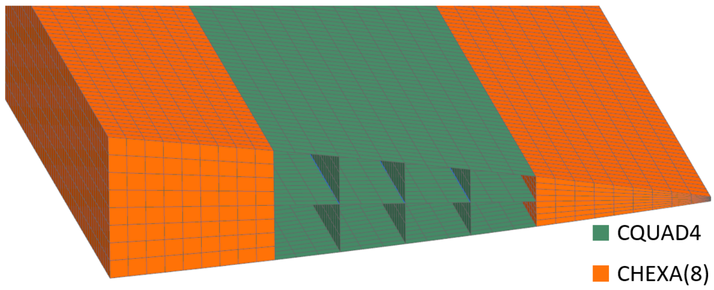

Figure 3: Mesh used with CQUAD4 and CHEXA(8) elements.

The material assigned to the mesh of the rigid non-morphing parts was aluminium 2014-O. For the 2D mesh representing the stringers, the material assigned was the Ninjatek Armadillo TPU. For the representative mesh of the skin, the Ninjatek Ninjaflex TPU was used. Finally, for the spine, a 2D mesh with the physical properties of a laminated composite material was used. This composite material was defined using the stacking sequence of [90/90/0/90/90] with five plies of 8552/IM7 Unidirectional (UD) carbon fiber prepreg with a total thickness of 0.65 mm.

The used mechanical properties, listed in Table 1, were taken from the database in MatWeb (2022) (aluminium 2014-O) and from the results of the mechanical tests presented by Rivero et al. (2022).

Table 1: Summary of material properties of the third generation of the FishBAC (Rivero et al., 2022).

Material	8552/IM7	Armadillo	Ninjaflex	Aluminum 2014-O
E_{11}	168.91 GPa			
E_{22}	8.00 GPa	275 MPa	15.3 MPa	72.4 GPa
E_{33}	8.00 GPa			
G_{12}	4.79 GPa			
G_{13}	4.79 GPa	97.0 MPa	5.50 MPa	28.0 GPa
G_{23}	2.76 GPa			
ν_{12}	0.32			
ν_{13}	0.32	0.42	0.39	0.33
ν_{23}	0.45			

3.2.2 Boundary conditions and Applied loads

In order to perform the simulations related to the structural analysis it is necessary to define the boundary conditions to be applied to the model. The only constraint applied was to fix all the degrees of freedom of the rigid part that is closer to the leading edge of the wing, marked in orange colour in Figure 3.

Regarding the loads applied, torque is applied to the spine, in the nodes that are closest to the three locations where the tendons anchors were connected to the spine, considering the third generation model FishBAC presented by Rivero et al. (2022). The initial value used was 4 Nm, applied in the direction that makes the trailing edge deflect downwards, in the negative direction of the global y-axis. It is also important to mention that this value of 4 Nm was used as it gave useful levels of deflection while still being in the range of what is achievable from commercially available servo actuators. The baseline and the models studied were also tested using an applied torque of 1 Nm and 10 Nm.

Lastly, Glue Connections were used to ensure that the 2D Laminate elements were secured to the 3D solid elements. The rest of the elements were connected using the sew function available in the software.

3.2.3 Verification and Validation

Figure 4 presents the values of deflection of the trailing edge, in the negative direction of the global y-axis, along the spanwise direction. It is possible to clearly see three vertices in the location where the torques (T) were applied. This corresponds to the location of the actuators that have as coordinates 99.5 mm, 497.5 mm and 895.5 mm in the spanwise direction.

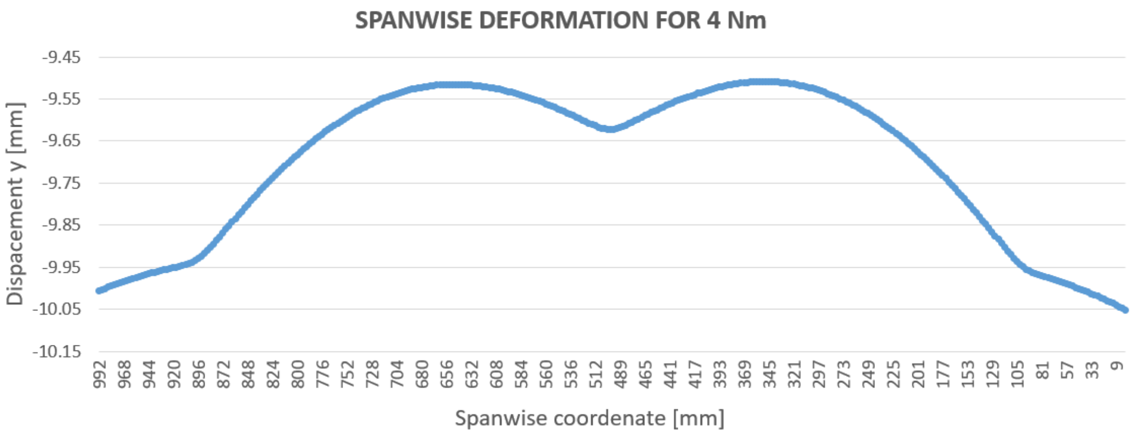

Figure 4: Spanwise deformation of the trailing edge for a T of 4 Nm.

The displacement of the trailing edge at the span midpoint ($w_{s/2}$) was 9.62 mm. This level of deflection is reasonable as it allows for significant variation of the lift coefficient (C_L) with a modest impact on drag, which is the intention for this type of morphing device, as referred by Woods, Fincham, and Friswell (2014).

The shape of the spanwise deformation is not perfectly symmetric as it can be seen in Figure 4. This is understandable because the order of magnitude of the difference in the values of the deformation, considering two symmetric locations, is about 10^{-2} mm. While the exact cause of the asymmetry in the response is not known for certain, it is likely due to either inconsistency in the mesh or perhaps some other form of numerical inconsistency. While not ideal, the overall deformation values are much higher than the asymmetries in the deformation, and the spanwise variation is also significantly larger than the asymmetry, allowing the possibility to meaningfully consider the impact of design changes on the overall deformation and its spanwise variation, despite the asymmetry.

3.3 Mesh Convergence Test

It was necessary to perform a mesh convergence study, to ascertain the best compromise between the number of elements and computation cost. The initial element base size was 3 mm and the results were validated as described in the previous chapter.

From this, the element size was reduced in half (1.5 mm) for all the components, keeping the relative size of the elements similar and their geometry constant, in order to obtain consistent results between the various simulations. Similar processes were made but to obtain less refined meshes with twice (6 mm) and triple (9 mm) the base size of the initial 3 mm value considered. The results of these simulations are summarized in Table 2.

Table 2: Mesh converging Test

Nº Elements	Computing time [seg]	$w_{s/2}$ [mm]	Relative difference [%]
4662	9.01	7.97	-
16932	18.34	15.16	47.39
64408	57.67	9.62	57.51
257244	251.89	17.10	43.72

It was possible to verify that, the simulation runtime for 1.5 mm was more than four times bigger than the computing time obtain for the 3 mm mesh. For the 6 mm simulation, the computational time was more than three times quicker than the time obtain for the 3 mm mesh and for the 9 mm mesh, more than six times.

The absolute relative differences have really high values when compared to the intended value defined as converging criteria (less than 5%).

While the results of the mesh convergence study were somewhat inconclusive due to potential inconsistencies in the implementation of the different mesh sizes, the 3 mm mesh was chosen as it still provided the most useful balance of resolution and solution time.

3.4 Prameters to study the elastic washout

The first parameter that is defined to evaluate elastic washout is the difference between maximum and minimum values of trailing edge displacement, normalised by the average displacement obtained (Δ_{norm}). This is a dimensionless value and can be given by Equation 1.

$$\Delta_{norm} = \frac{|w_{max} - w_{min}|}{\bar{w}}. \tag{1}$$

The second parameter studied is the standard deviation (σ_P) that is applied to all registered values of trailing edge displacement along the span. This parameter is expressed in mm and can be defined by Equation 2.

$$\sigma_P = \sqrt{\frac{\sum(w - \bar{w})^2}{n}}. \tag{2}$$

The letter n represents the total number of points there is in the dataset that this formula is applied to, equal, in this case, to the number of mesh nodes along the trailing edge. These parameters were evaluated for the baseline model and also for the A1, B1 and model that combines the A1 and B1 models.

The information obtained for the baseline model was important to draw conclusions about the A1, B1 and the combined models, as it is used as a reference for the T sweep condition.

4 Model A1

The A1 model was defined starting from the baseline model and making rectangular cutouts. For this model, the cutouts were designed to remove only 80% of the spine in the chord-wise direction. Considering the spine chord-wise direction length of 40.5 mm, the length of the cutout in that direction is 32.4 mm.

The same was defined for the span-wise direction but different percentages were studied (25%, 50% and 75%). For example, figure 5 shows part of the spine with cutouts configuration for 50% removal of the material in the chordwise direction. The pink dotted line represents the midpoint of the spine and the symmetry axis. This means that the represented spine cutouts are exactly equal to the other side of the spine, which is not represented in the picture.

The red line is positioned parallel to the symmetry axis and passes through the location of the outer actuation point. It is important to mention that the pink dotted line passes through the location of the central actuation point. These lines are relevant because, by design, they are a reference to the location of the cutouts in the spanwise direction. For example, the cutout located at the left side of the red line has its center located at 40% distance from the red line, considering the length that goes from the left side of the spine to the red line.

The other two cutouts, which are placed between the red and pink lines, have their center located so that the distance between both is twice the distance that separates the center of the cutout and the closest line (pink or red).

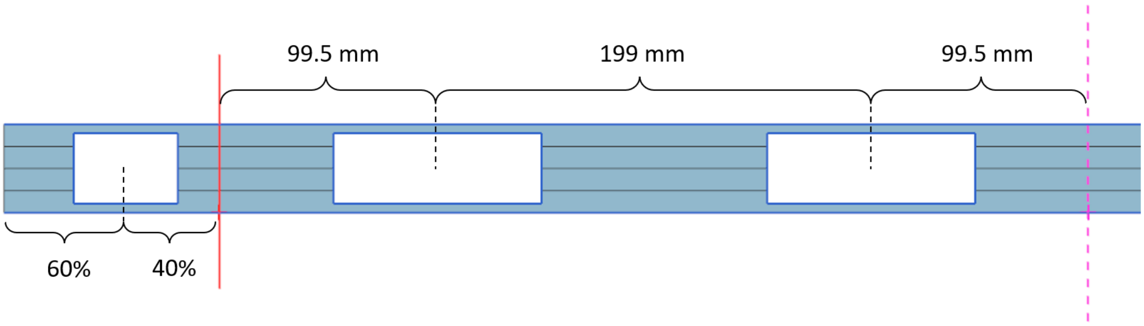

Figure 5: Midspan Cutouts Configuration.

4.1 Results

The obtained results for the span-wise displacement with relation to the different percentages of material removed are summarised in Table 3.

Table 3: Results for the span-wise displacement with relation to the different percentages of material removed.

% of material removed in spanwise direction	T [Nm]	$w_{s/2}$ [mm]	$T/w_{s/2}$ [Nm/mm]	Δ_{norm} [%]	Δ_{norm} difference to baseline. [%]	σ_P [mm]
0	1	2.41		5.60	-	0.05
0	4	9.62	2.41	5.60	-	0.18
0	10	24.06		5.60	-	0.45
25	1	3.79		5.32	-0.27	0.06
25	4	15.15	3.79	5.32	-0.27	0.23
25	10	37.86		5.32	-0.27	0.57
50	1	4.91		5.81	0.21	0.08
50	4	19.63	4.91	5.81	0.21	0.33
50	10	49.06		5.81	0.21	0.82
75	1	6.37		8.57	2.98	0.16
75	4	25.47	6.37	8.57	2.98	0.63
75	10	63.68		8.57	2.98	1.57

It is possible to observe from the data presented in Table 3 that, for the case of the 25% of material removed, the Δ_{norm} difference to the baseline model is almost zero. The same can be said for the case of 50% of material removed. Nevertheless, the model that has 75% of the spine removed in the spanwise direction, presents a significantly higher value of Δ_{norm}. This indicates that the use of cutouts do not have a significant effect in the deflection variation for value from zero to a certain point where this effect starts to appear.

Looking at the standard deviation results (σ_P) for the models studied in this chapter, independently of percentages of material removed, the σ_P is always higher than the σ_P obtained for the baseline model.

Another fact that can be stated from the data in Table 3 is that the cutouts with values of Δ_{norm} closest to the value present by the baseline model is the 50% of removed material (Δ_{norm} difference to baseline ≈ 0). This model also presents high values for the difference between the model σ_P of the baseline when compared to the same value for 25% but, significantly lower when compared to the ones presented by the 75% model.

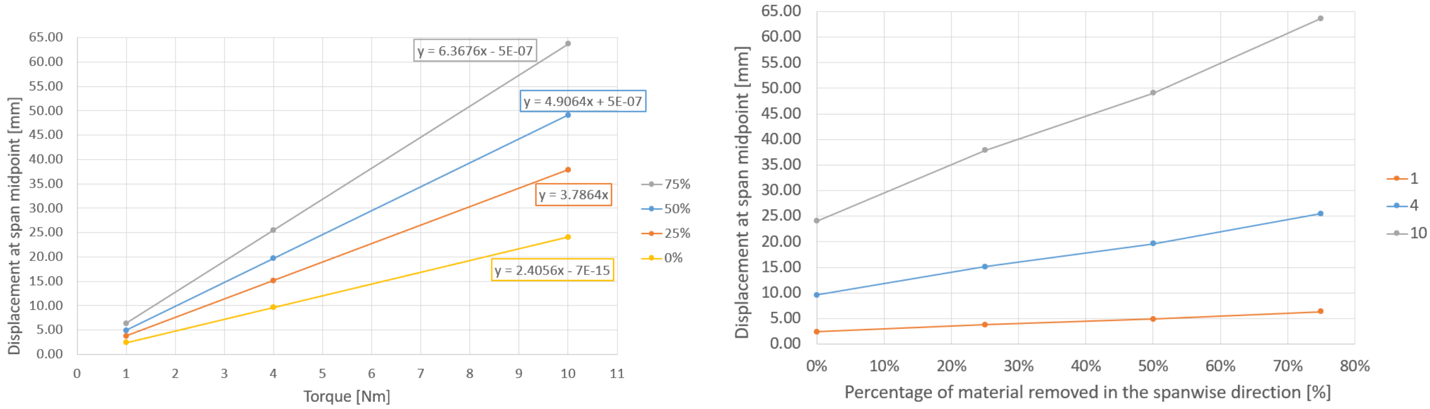

(a) Displacement measured at the span midpoint in function of the applied T.

(b) Effect of the cutouts in the displacement at span midpoint for different values of applied T.

Figure 6: Graphic representations of the results for the model A1.

In Figure 6 (a) it can be seen that for the same applied T, the displacement for the span midpoint increases with the increase of the percentage of material removed. This behavior was expected because, by removing material from the spine, we are decreasing the stiffness of the material allowing it to be more easily bent and achieve higher displacements. This is also confirmed by the slopes of the lines that represent the percentage of material removed. For a cutout with higher dimensions, the trailing edge reaches a specific deflection with less applied T. This reduction in the applied T, with the increase of the dimension of the cutouts, can be translated into less energy needed for the FishBAC device to function, with a reduced weight associated.

Figure 6 (b) shows the effect of the dimension of the cutouts in the trailing edge displacement at the span midpoint, for different values of applied T. This representation can be used to estimate what will be the values of the trailing edge displacement for a given percentage of material removed, for the values of applied T and even for the values between. This can be used as a reference to begin the process of designing a FishBAC device.

Taking all of this into consideration, it is possible to say that 50% cutout configuration seems to provide the best balance of less rigidity, requiring less T for a specific displacement and does not have a significant high elastic washout effect.

The full impact of removing spine material should ultimately be considered in an aeroelastic sense, in order to make sure that the reduced stiffness does not lead to any undesired aeroelastic phenomena, but that falls outside the scope of the present work.

5 Model B1

Model B1 which includes the CFRP pultrusions was designed using lines defined by interception of the 2D planes that correspond to the stringers and skin components. In the creation of the 1D mesh for the pultrusion, the element selected was the CBAR. The CBAR element is a beam type element that supports tension and compression, torsion, bending in two perpendicular planes, and shear in two perpendicular planes, adequate for the testing. In this step, the PBARL was used to define the physical properties of the pultrusion material. The cross-section shape used was the square and 1 mm, 2 mm and 3 mm were the side dimension studied.

The material properties values used for the CFRP pultrusions were taken from Agarwal, Broutman, and Chandrashekhara (2017). The material was defined as isotropic which, in this case, it is acceptable, considering that the pultrusion will act primarily as an axially loaded member, with transverse strains and stresses, not having a first order impact on the overall stiffness of the FishBAC.

5.1 Results

The obtained results for the span-wise displacement with relation to the different CFRP pultrusion are summarised in Table 4. It is important to mention that the added mass that appears in Table 4 accounts for the mass of the CFRP pultrusions.

Table 4: Results for the span-wise displacement with relation to the dimension of the cross-section of the Square pultrusion.

Dimension of cross-section Square pultrusion [mm]	T [Nm]	$w_{s/2}$ [mm]	Δ_{norm} [%]	Δ_{norm} difference to baseline. [%]	σ_P [mm]	Added Mass [g]	Reduction of Normalized dif. / Added Mass [%/g]
0	1	2.41	5.60	-	0.05	-	-
0	4	9.62	5.60	-	0.18	-	-
0	10	24.06	5.60	-	0.45	-	-
1	1	2.41	5.31	-0.28	0.04	1.60	-0.18
1	4	9.63	5.31	-0.28	0.18	1.60	-0.18
1	10	24.07	5.31	-0.28	0.44	1.60	-0.18
2	1	2.41	5.25	-0.34	0.04	6.41	-0.05
2	4	9.62	5.25	-0.34	0.18	6.41	-0.05
2	10	24.06	5.25	-0.34	0.44	6.41	-0.05
3	1	2.41	5.19	-0.41	0.04	14.42	-0.03
3	4	9.62	5.19	-0.41	0.17	14.42	-0.03
3	10	24.06	5.19	-0.41	0.44	14.42	-0.03

The model that uses the pultrusion with a 3×3 mm^2 squared cross-section has, as seen in Table 4, the lowest value of Δ_{norm}. This is also true for the σ_P. Considering this, it is possible to say that the higher the cross-section of the pultrusion, the less variation in the displacement of the trailing edge is registered. This behaviour was expected since the pultrusions are made of highly rigid materials when compared to the materials used in the skin and stringer, having more capacity to distribute the loads along the span, when compared to skin and stringer without this feature.

Both σ_P and Δ_{norm} with the increase of the dimensions of the cross-section of the square pultrusion, have a really modest negative tendency. This support the affirmation that the added pultrusions have less of an effect on preventing the elastic washout to happen, with only a very modest reduction in the variation of the trailing edge deflection along the span. This can be the real behavior of a model with these features but, it can not be excluded that the modeling approach can also be influencing these results.

6 Combination of model A1 and B1

Considering the promising results obtained for the previously studied models, a third model that combines the two other was created and studied. The configurations studied are listed in Table 5.

The model with cutouts that removed 50% of material in the spanwise direction was selected because it presented the best trade-off between the quantity of material removed and the percentage of the variation in displacement along the span.

The model with 75% of material removed was also selected in order to understand if the pultrusion could affect the really high variation shown in Table 3. The expected results for the combination of this cutout model with CFRP pultrusions is to lower the values of variation in trailing edge displacement. It was analysed if the respective results could be approximated to the one obtained for the model with no cutouts.

6.1 Results

The obtained results for the combined model are presented in Table 5.

Table 5: Obtained results from Model combining A1 and B1

% of material removed in spanwise direction [%]	Dimension of the cross-section of Square pultrusion [mm]	T [Nm]	$w_{s/2}$ [mm]	Δ_{norm} [%]	Δ_{norm} difference to baseline. [%]	σ_P [mm]	Added Mass [g]	Reduction of Normalized dif. / Added Mass [%/g]	Reduction of the σ_P / Added Mass [%/g]
50	1	1	4.88	5.73	0.13	0.08	1.60	0.08	48.16
50	1	4	19.53	5.73	0.13	0.32	1.60	0.08	48.16
50	1	10	48.83	5.73	0.13	0.80	1.60	0.08	48.16
50	2	1	4.87	5.54	-0.06	0.08	6.41	-0.01	11.25
50	2	4	19.50	5.54	-0.06	0.31	6.41	-0.01	11.25
50	2	10	48.74	5.54	-0.06	0.78	6.41	-0.01	11.25
75	1	1	6.34	8.32	2.72	0.15	1.60	1.70	144.08
75	1	4	25.38	8.32	2.72	0.60	1.60	1.70	144.08
75	1	10	63.44	8.32	2.72	1.49	1.60	1.70	144.08
75	2	1	6.34	8.00	2.40	0.14	6.41	0.37	33.43
75	2	4	25.38	8.00	2.40	0.57	6.41	0.37	33.43
75	2	10	63.45	8.00	2.40	1.42	6.41	0.37	33.43

From the data presented in table 5 it is possible to state that both types of pultrusions tested in the combination with cutouts with 75% material removed have reduced the variation in the displacement. Although, this reduction was not significant to be approximated to the results obtained for the model with no cutouts, not meeting the expectations defined in the chapter 6. Even though, is important to mention that the CFRP pultrusions with 2 mm squared cross-ection had better results when compared to the ones obtained for 1 mm.

A major conclusion of the combined model study is that applying 2 mm pultursions in the model with the 50% cutout gives an outstanding result that is capable of achieving twice the trailing edge deflection verified in the baseline model (48.74 mm vs 24.06 mm) and also a slightly improve the displacement variation in spanwise direction (5.54% vs 5.6%).

7 Conclusions

The main objective of this dissertation was to propose new structural solutions that could respond to the limitations of the existing model of the FishBAC device.

With the conceptual ideas established, a decision process was used in order to choose the concepts that were more promising to better respond to the improving objectives of the FishBAC. From this step, it was concluded that the modifications to be studied were the introduction of cutouts in the spine (Model A1) and the reinforcement of the stringers, next to the skin, using CFRP pultrusions (Model B1).

Then, a CAD model representation of the FishBAC was designed. The FEA was applied to this model, the respective results were registered and later used as the baseline of the study of the modifications. A mesh convergence test was conducted. From this, it was concluded that the mesh did not converge.

The results obtained for model A1 helped to conclude that, removing some of the spine's material in rectangular cutouts can reduce the total mass and energy required to achieve a specific deflection. One other conclusion possible for this modification was that the use of cutouts reduces the bending stiffness of the device, increasing displacement at a given T. But, if too much is removed, a higher % variation in displacement along the span starts to occur. The cutouts that remove 50% of the spine in the spanwise direction seem to provide the best balance of these factors.

Regarding model B1 it was concluded that introducing CFRP pultrusion connected to the stringer, next to the skin, has a minor but positive effect in the reduction of the spanwise variation.

As conclusions for the combination of the models A1 and B1, it was found that combining 2 mm pultrusions in the model with the 50% cutout in the spanwise direction, gives a model that has less rigidity, that can deliver a deflection that is two times more than the deflection obtained for the baseline model. This configuration of pultrusion and cutouts was found to have less variation in the spanwise direction. It was also concluded that this model (2 mm pultrusions in the model with the 50% cutout) is also the one that shows the lowest value, from the studied ones, for the parameters that are related to the added mass (reduction of the Δ_{norm} divided by the added mass and reduction of the σ_P divided by the added mass).

The continuation of this work will be important to help the evolution of the FishBAC in terms of performance and efficiency in the achievement of the design objectives of this type of camber morphing device. To overcome some of the limitations encountered it is proposed to redo the process of generating the mesh and the converging test. It is also crucial to study an effective way for the insertion of the CFRP pultrusions next to skin and stringers. Another possible work to be done is to do a study of other types of shapes for the cutouts and cross-section of the pultrusions. An economic, maintenance and operation study, to assess the potential of the solutions proposed, can be a future work that could help the implementation of this technology in real operating aircraft wings. Finally, it is suggested to do a real-life application of the model, by building a prototype and do a real mechanical test to validate the results obtained and the drawn conclusions.

References

Agarwal, B. D., Broutman, L. J., & Chandrashekhara, K. (2017). *Analysis and performance of fiber composites*. Wiley.

Airfoil Tools. (2022). *Naca 23012 12% (naca23012-il).* Retrieved 2022-07-26, from `http://airfoiltools.com/airfoil/details?airfoil=naca23012-il`

Burdette, D. A., & Martins, J. R. R. A. (2019). Impact of morphing trailing edges on mission performance for the common research model. *Journal of Aircraft*, *56*, 369-384. doi: 10.2514/1.C034967

Greff, E. (1990). The development and design integration of a variable camber wing for long/medium range aircraft. *The Aeronautical Journal (1968)*, *94*(939), 301–312. doi: 10.1017/S0001924000023186

MatWeb. (2022). *Aluminum 2014-o.* Retrieved 2022-07-28, from `https://www.matweb.com/search/DataSheet.aspx?MatGUID=3380dbc77437443b9674c6da219bd664&ckck=1`

Rivero, A. E., Fournier, S., Heeb, R., & Woods, B. K. S. (2022, January). Design, manufacture and wind tunnel test of a modular fishbac wing with novel 3d printed skins. *Applied Sciences (Switzerland)*, *12*. doi: 10.3390/app12020652

Rivero, A. E., Fournier, S., Manolesos, M., Cooper, J., & Woods, B. K. S. (2020, January). Wind tunnel comparison of flapped and FishBAC camber variation for lift control. In AIAA Scitech 2020 Forum (Ed.), . Orlando, FL: American Institute of Aeronautics and Astronautics, Inc. doi: 10.2514/6.2020-1300

Rivero, A. E., Fournier, S., Manolesos, M., Cooper, J. E., & Woods, B. K. S. (2021, July). Experimental aerodynamic comparison of active camber morphing and trailing-edge flaps. *AIAA Journal*, *59*, 2627-2640. doi: 10.2514/1.J059606

Rivero, A. E., Fournier, S., Weaver, P., Cooper, J. E., & Woods, B. K. S. (2018, October). Manufacturing and characterisation of a composite FishBAC morphing wind tunnel model. In 29th International Conference on Adaptive Structures and Technologies, ICAST 2018 (Ed.), . Retrieved from `http://www.icast2018.com`

Rivero, A. E., Weaver, P., Cooper, J. E., & Woods, B. K. S. (2018, May). Parametric structural modelling of fish bone active camber morphing aerofoils. *Journal of Intelligent Material Systems and Structures*, *29*, 2008-2026. doi: 10.1177/1045389X18758182

Woods, B. K. S., Fincham, J. H. S., & Friswell, M. I. (2014). Aerodynamic modelling of the fish bone active camber morphing concept. In *Proceedings of the raes applied aerodynamics conference, bristol, uk* (Vol. 2224).

Woods, B. K. S., & Friswell, M. I. (2012, September). Preliminary investigation of a fishbone active camber concept. In *Volume 2: Mechanics and behavior of active materials integrated system design and implementation bio-inspired materials and systems energy harvesting.* American Society of Mechanical Engineers. Retrieved from https://doi.org/10.1115/smasis2012-8058 doi: 10.1115/smasis2012-8058

Woods, B. K. S., & Friswell, M. I. (2013, April). Fluid-structure interaction analysis of the fish bone active camber mechanism. In *54th AIAA/ASME/ASCE/AHS/ASC structures, structural dynamics, and materials conference.* American Institute of Aeronautics and Astronautics. Retrieved from https://doi.org/10.2514/6.2013-1908 doi: 10.2514/6.2013-1908